Science Advances

AAAS

advances.sciencemag.org/cgi/content/full/4/6/eaar6327/DC1

Supplementary Materials for

Experimental benchmarking of quantum control in zero-field nuclear magnetic resonance

Min Jiang, Teng Wu, John W. Blanchard, Guanru Feng, Xinhua Peng, Dmitry Budker

Published 15 June 2018, *Sci. Adv.* **4**, eaar6327 (2018)
DOI: 10.1126/sciadv.aar6327

This PDF file includes:

- Supplementary Materials and Methods
- section S1. Hamiltonians and eigenstates
- section S2. State tomography
- section S3. Single-spin control
- section S4. Two-spin control via CNOT gate
- table S1. The evolutions of two-spin operators under the scalar spin-spin coupling.
- table S2. Temporal averaging sequences for state tomography.
- table S3. The evolution of the two-spin operators under the CNOT gate.
- table S4. Reconstructing the CNOT gate based on *l*-norm.
- fig. S1. Experimental realization of temporal averaging.
- fig. S2. Dependence of NMR signal amplitude on *z* pulse duration.

Supplementary Materials and Methods

section S1. Hamiltonians and eigenstates

The Hamiltonian for two coupled heteronuclear spins, $\mathbf{I}$ and $\mathbf{S}$, at zero magnetic field is: $H_J = 2\pi J \mathbf{I} \cdot \mathbf{S}$, where J is the strength of the scalar spin-spin coupling. In the high-field limit, the eigenstates are those of I_z and S_z, i.e., $\{|\uparrow\uparrow\rangle, |\uparrow\downarrow\rangle, |\downarrow\uparrow\rangle, |\downarrow\downarrow\rangle\}$. At zero field, the eigenstates are a singlet and a triplet. We denote the singlet state with $F = 0$ as $|S_0\rangle$, and the triplet state with $F = 1$ as $|T_{+1,0,-1}\rangle$, which have the forms as follows:

$$
\begin{aligned}
|S_0\rangle &= (|\uparrow\downarrow\rangle - |\downarrow\uparrow\rangle)/\sqrt{2} \qquad & E_{|S_0\rangle} &= -\frac{3\pi J}{2} \\
|T_{+1}\rangle &= |\uparrow\uparrow\rangle & E_{|T_{+1}\rangle} &= \frac{\pi J}{2} \\
|T_0\rangle &= (|\uparrow\downarrow\rangle + |\downarrow\uparrow\rangle)/\sqrt{2} \qquad & E_{|T_0\rangle} &= \frac{\pi J}{2} \\
|T_{-1}\rangle &= |\downarrow\downarrow\rangle & E_{|T_{-1}\rangle} &= \frac{\pi J}{2}
\end{aligned}
$$

section S2. State tomography

The quantum state of a nuclear-spin system can be described by the density matrix ρ, which can be characterized by state tomography (*31*). For the sake of abbreviation in notation, the density matrix ρ can be expressed in the Pauli basis as $\rho = \mathbf{I} \cdot V \cdot \mathbf{S}$, where $\mathbf{S} = [\mathbb{1}, S_x, S_y, S_z]^T$, $\mathbf{I} = [\mathbb{1}, I_x, I_y, I_z]$, and $V_{\nu\mu}$ of the matrix V represents the coefficient of $I_\nu S_\mu$ term ($\nu, \mu = 0, 1, 2, 3$). State tomography consists of measuring the matrix V, or the coefficients of the fifteen nontrival $I_\nu S_\mu$ terms ($I_0 S_0 = \mathbb{1}$ is an identity matrix). The sixteen $I_\nu S_\mu$ terms can be expressed in the Pauli matrices (σ_x, σ_y, and

σ_z) and have the forms as follows.

$$
\begin{array}{lll}
\mathbb{1} = \mathbb{1}_{2\times2} \otimes \mathbb{1}_{2\times2} & & \\
I_x = \frac{1}{2}\sigma_x \otimes \mathbb{1}_{2\times2} & I_y = \frac{1}{2}\sigma_y \otimes \mathbb{1}_{2\times2} & I_z = \frac{1}{2}\sigma_z \otimes \mathbb{1}_{2\times2} \\
S_x = \mathbb{1}_{2\times2} \otimes \frac{1}{2}\sigma_x & S_y = \mathbb{1}_{2\times2} \otimes \frac{1}{2}\sigma_y & S_z = \mathbb{1}_{2\times2} \otimes \frac{1}{2}\sigma_z \\
I_xS_x = \frac{1}{2}\sigma_x \otimes \frac{1}{2}\sigma_x & I_xS_y = \frac{1}{2}\sigma_x \otimes \frac{1}{2}\sigma_y & I_xS_z = \frac{1}{2}\sigma_x \otimes \frac{1}{2}\sigma_z \\
I_yS_x = \frac{1}{2}\sigma_y \otimes \frac{1}{2}\sigma_x & I_yS_y = \frac{1}{2}\sigma_y \otimes \frac{1}{2}\sigma_y & I_yS_z = \frac{1}{2}\sigma_y \otimes \frac{1}{2}\sigma_z \\
I_zS_x = \frac{1}{2}\sigma_z \otimes \frac{1}{2}\sigma_x & I_zS_y = \frac{1}{2}\sigma_z \otimes \frac{1}{2}\sigma_y & I_zS_z = \frac{1}{2}\sigma_z \otimes \frac{1}{2}\sigma_z
\end{array}
$$

As mentioned above, the coefficient of $I_\nu S_\mu$ can be extracted by measuring both the amplitude and phase of the oscillating magnetization signal generated from its evolution under H_J. Since our magnetometer is sensitive to the magnetic field along the z axis, only the z component of the magnetization signal is detected. According to the calculation results in table S1, there are only four terms, I_z, I_yS_x, I_xS_y and S_z, that can generate oscillating magnetization signal along the z axis. The experimental-observable operator of the atomic magnetometer can be written as $\hat{\mathcal{O}} = \gamma_I I_z + \gamma_S S_z$. The observable NMR signal is the z magnetization, and has the form as $M_z \propto \mathrm{Tr}(\rho\hat{\mathcal{O}})$. The coefficients of the other terms can only be measured after applying additional operations and to transform them into one of the four observable terms. Since all the four observable terms can generate signals along the z axis, it is impossible to determine the coefficient for each of them with a single measurement. To solve these problems, we implement a temporal averaging method (*19*), which averages the results of four experiments. For each measurement, a pulse sequence ($\mathcal{P}_i$, where i refers to the ith measurement) is specially designed to change the signs of some coefficients, while having no effect on the sign of the coefficient we need to measure. The signal amplitude in the averaged spectrum is then proportional to the coefficient to be measured, and independent of all others.

To illustrate the details of our approach, we present an example of determining the coefficient

of S_z term (V_{30}) in the density matrix ρ of the initial state. Four independent experiments are performed with different pulse sequences, which are summarized in table S2. Generally speaking, $\mathcal{P}_1$ is no operation, and the measured result is a linear combination of the four coefficients, V_{30}, V_{21}, V_{12}, V_{03}. In order to determine the value of V_{30} individually, $\mathcal{P}_2$, $\mathcal{P}_3$, $\mathcal{P}_4$ are specially designed to change the sign of specific coefficients, which are shown below

$$\mathcal{P}_1\rho\mathcal{P}_1^\dagger = \begin{pmatrix} & & & V_{03} \\ & & V_{12} & \\ & V_{21} & & \\ V_{30} & & & \end{pmatrix} + \mathcal{A}_1,$$

$$\mathcal{P}_2\rho\mathcal{P}_2^\dagger = \begin{pmatrix} & & & V_{03} \\ & & -V_{12} & \\ & -V_{21} & & \\ V_{30} & & & \end{pmatrix} + \mathcal{A}_2,$$

$$\mathcal{P}_3\rho\mathcal{P}_3^\dagger = \begin{pmatrix} & & & -V_{03} \\ & & -V_{12} & \\ & V_{21} & & \\ V_{30} & & & \end{pmatrix} + \mathcal{A}_3,$$

$$\mathcal{P}_4\rho\mathcal{P}_4^\dagger = \begin{pmatrix} & & & -V_{03} \\ & & V_{12} & \\ & -V_{21} & & \\ V_{30} & & & \end{pmatrix} + \mathcal{A}_4$$

where $\mathcal{A}_i$ ($i = 1, 2, 3, 4$) is a matrix where all the anti-diagonal elements are zero and other elements are equal to the corresponding elements in $\mathcal{P}_i\rho\mathcal{P}_i^\dagger$. In our analysis, we neglect $\mathcal{A}_i$ because $\mathcal{A}_i$ can not generate an observable signal under the evolution governed by H_J. Consequently, by averaging the results of the four experiments, $\rho_{\text{ave}} = \sum_i \mathcal{P}_i\rho\mathcal{P}_i^\dagger = 4V_{30}S_z$, one can determine the coefficient V_{30} of the S_z term. Similar approach can be used in determining other $I_\nu S_\mu$ terms in density matrix ρ, of which the pulse sequences are summarized and shown in table S2.

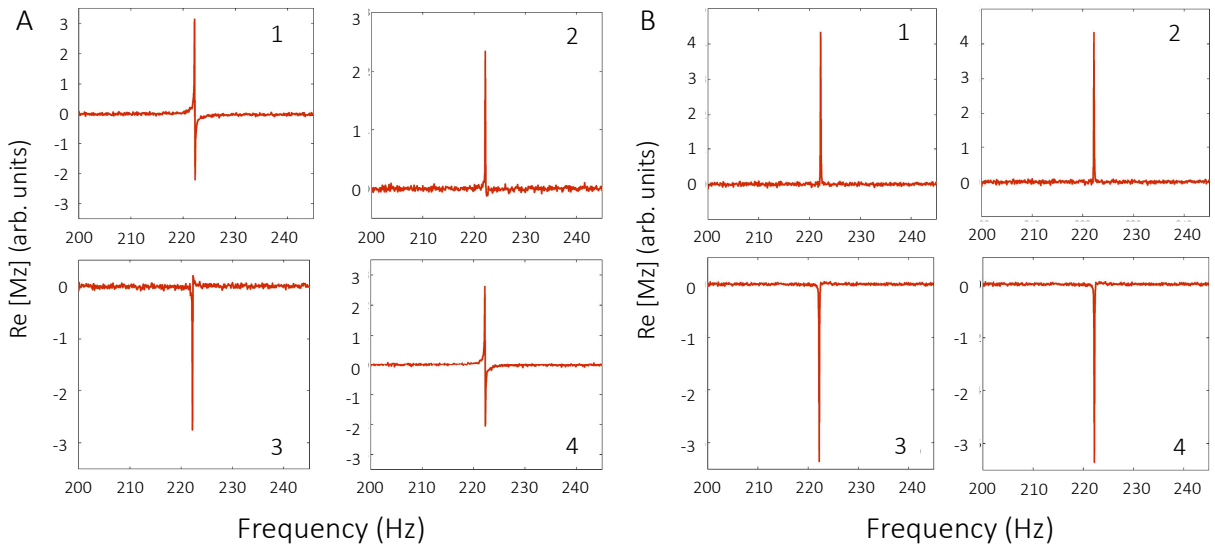

fig. S1. Experimental realization of temporal averaging. (**A**) Experimental results of temporal averaging for I_xS_x in the adiabatic state. (1), (2), (3), and (4) denote the measured signal by applying preparation operation $\mathcal{P}_1$, $\mathcal{P}_2$, $\mathcal{P}_3$ and $\mathcal{P}_4$ (see table S3, I_xS_x), respectively. The average result of (1-4) is equal to the coefficient of I_xS_x. (**B**) Experimental results of temporal averaging for S_z in the sudden state. (1), (2), (3), and (4) denote the measured signal by applying preparation operation $\mathcal{P}_1$, $\mathcal{P}_2$, $\mathcal{P}_3$ and $\mathcal{P}_4$ (see table S3, S_z), respectively. The average result of (1-4) is equal to the coefficient of S_z.

We demonstrate the use of our approach to reconstruct quantum states, or the controlled density matrix of the experimentally realized sudden and adiabatic states. The forms of the theo retically expected sudden and adiabatic states are presented in the main text. For instance, fig. S1A shows the temporal averaging result of I_xS_x of the experimentally realized adiabatic state, and fig. S1B shows the temporal averaging result of S_z of the experimentally realized sudden state. According to table S2, I_xS_x is not observable under the evolution governed by H_J. In order to measure its coefficient, as shown in table S2, a $\frac{\pi}{2}$ pulse along z axis $([\frac{\pi}{2}]_S^z)$ is applied to the spin $\mathbf{S}$ (^{13}C) to transform I_xS_x into I_xS_y, which is observable. table S2 also shows that the observable signals generated by I_xS_y and S_z have $\frac{\pi}{2}$ phase difference: if the real part of the signal from S_z is absorptive, it should be dispersive for I_xS_y. Indeed, this agrees well with the results shown in fig. S1A. By adding the results of the four experiment for each term, the state-tomography results for

the two states are:

$$\rho_{\text{adiabatic}} = \begin{array}{c} \begin{matrix} \mathbb{1} & I_x & I_y & I_z \end{matrix} \\ \begin{bmatrix} 0 & -0.24(6) & -0.24(6) & \mathbf{2.23}(6) \\ -0.17(3) & \mathbf{-3.9}(3) & 0.04(4) & -0.3(1) \\ -0.05(2) & 0.08(4) & \mathbf{-4.6}(3) & 0.3(1) \\ \mathbf{2.48}(5) & 0.30(4) & -0.04(5) & 0.8(4) \end{bmatrix} \end{array} \begin{matrix} \mathbb{1} \\ S_x \\ S_y \\ S_z \end{matrix} ,$$

and

$$\rho_{\text{sudden}} = \begin{array}{c} \begin{matrix} \mathbb{1} & I_x & I_y & I_z \end{matrix} \\ \begin{bmatrix} 0 & 0.8(1) & -1.0(6) & \mathbf{57.9}(9) \\ 0.8(3) & 2.3(5) & -2(1) & -0.2(3) \\ 0.9(6) & 2(1) & -2.4(8) & 2.6(8) \\ \mathbf{14}(1) & 3(1) & -1.3(4) & -1.1(9) \end{bmatrix} \end{array} \begin{matrix} \mathbb{1} \\ S_x \\ S_y \\ S_z \end{matrix}$$

where the coefficient of $\mathbb{1} \otimes \mathbb{1}$ term is defined as $V_{00} = 0$ because this term is not observable. The values in the state-tomography matrix are the corresponding signal amplitude for each term, of which the sign is calibrated with I_z and S_z. The results of $\rho_{\text{adiabatic}}$ and ρ_{sudden} can be rewritten in the computational basis (0_I0_S,0_I1_S,1_I0_S, and 1_I1_S, here $|0\rangle = |\uparrow\rangle$ and $|1\rangle = |\downarrow\rangle$),

$$\rho_{\text{adiabatic}} = \begin{array}{c} \begin{matrix} 0_I0_S & 0_I1_S & 1_I0_S & 1_I1_S \end{matrix} \\ \begin{bmatrix} 2.56 & -0.16 - 0.06\text{i} & -0.05 + 0.13\text{i} & 0.18 - 0.03\text{i} \\ -0.16 + 0.06\text{i} & -0.32 & -2.11 + 0.01\text{i} & -0.20 + 0.11\text{i} \\ -0.05 - 0.13\text{i} & -2.11 - 0.01\text{i} & -0.07 & -0.002 + 0.11\text{i} \\ 0.18 + 0.03\text{i} & -0.20 - 0.11\text{i} & -0.002 - 0.11\text{i} & -2.16 \end{bmatrix} \end{array} \begin{matrix} 0_I0_S \\ 0_I1_S \\ 1_I0_S \\ 1_I1_S \end{matrix}$$

and

$$\rho_{\text{sudden}} = \begin{array}{c} \begin{matrix} 0_I0_S & 0_I1_S & 1_I0_S & 1_I1_S \end{matrix} \\ \begin{bmatrix} 35.76 & 0.35-1.04\text{i} & 1.00+0.80\text{i} & 1.18-0.20\text{i} \\ 0.35+1.04\text{i} & 22.14 & -0.04+0.98\text{i} & -0.25+0.17\text{i} \\ 1.00-0.80\text{i} & -0.04-0.98\text{i} & -21.56 & 0.45+0.19\text{i} \\ 1.18+0.20\text{i} & -0.25-0.17\text{i} & 0.45-0.19\text{i} & -36.33 \end{bmatrix} \end{array} \begin{matrix} 0_I0_S \\ 0_I1_S \\ 1_I0_S \\ 1_I1_S \end{matrix}$$

Accordingly, the fidelity of the state preparation is calculated as $f = \frac{\text{Tr}(\rho\rho_{\text{ideal}})}{\sqrt{\text{Tr}(\rho^2)}\sqrt{\text{Tr}(\rho_{\text{ideal}}^2)}} = 0.97(2), 0.99(1)$ for the experimentally realized adiabatic and sudden states. The forms of ρ_{ideal} or adiabatic and suddent states are presented in main text.

section S3. Single-spin control

The available external controls over nuclear spins are the magnetic-field pulses along x, y and z with the Hamiltonians $H_\eta = -B_\eta(\gamma_I I_\eta + \gamma_S S_\eta), \eta = x, y, z$. Here, $\mathbf{I}$ is ^{1}H and $\mathbf{S}$ is ^{13}C. As discussed in (*14*), an arbitrary rotation of one of the spins, for example, $\mathbf{I}$, can be realized by a composite pulse,

$$\mathcal{U}_\eta^I(\theta) = e^{-iI_\eta\theta} \approx \mathcal{U}_{\eta'}^S(\pi)e^{iH_\eta t_p/2}\mathcal{U}_{\eta'}^{S\dagger}(\pi)e^{iH_\eta t_p/2},$$

where $\theta = \gamma_I B_\eta t_p$ and $\eta \neq \eta'$. As an example, an arbitrary rotation along the x axis on spin $\mathbf{I}$ can be realized as follows: $\mathcal{U}_x^I(\theta) = e^{-iI_x\theta} = \mathcal{U}_z^S(\pi)e^{iH_x t_p/2}\mathcal{U}_z^{S\dagger}(\pi)e^{iH_x t_p/2}$, by using $Re^{iHt}R^\dagger = e^{iRHR^\dagger t}$ with a unitary operator R and its conjugation $R^\dagger$, e.g., $\mathcal{U}_z^S(\pi)S_x\mathcal{U}_z^{S\dagger}(\pi) = -S_x$ and $\mathcal{U}_z^S(\pi)I_x\mathcal{U}_z^{S\dagger}(\pi) = I_x$. The pulse sequences are of the same form for an arbitrary rotation along the y and z axis. Similarly, for the spin $\mathbf{S}$,

$$\mathcal{U}_\eta^S(\theta) = e^{-iS_\eta\theta} \approx \mathcal{U}_{\eta'}^S(\pi)e^{-iH_\eta t_p/2}\mathcal{U}_{\eta'}^{S\dagger}(\pi)e^{iH_\eta t_p/2}$$

Here, it should be pointed out the actual γ_I/γ_S is not perfectly equal to 4 but 3.977(2), i.e., the proton spin is rotated by 3.977π when the carbon spin is rotated by π angle. For example,

when the rotation is along the z axis, the ideal gate is $\mathcal{U}_z^S(\pi) = e^{-i4\pi I_z} \otimes e^{-i\pi S_z}$, while the actual gate is $\mathcal{U}_z^{'S}(\pi) = e^{-i3.977\pi I_z} \otimes e^{-i\pi S_z}$. The gate error caused by such a slight deviation can be estimated to be $1 - \mathrm{Tr}[\mathcal{U}_z^{'S}(\pi)\mathcal{U}_z^{\dagger S}(\pi)]/4 \approx 0.0006$, which is an order of magnitude smaller than the experimentally measured error.

section S4. Two-spin control via CNOT gate

In this work, the nuclear spin $\mathbf{I}$ (^{1}H) is chosen as the control spin and the nuclear spin $\mathbf{S}$ (^{13}C) is chosen as the target spin. The ideal controlled-not (CNOT) gate can be expressed in the computational basis (0_I0_S,0_I1_S,1_I0_S, and 1_I1_S), as shown in Matrix (1). To clarify the effect of the CNOT gate, we derive the transformation of the spin operator $I_\nu S_\mu$ after applying CNOT gate, as shown in table S3.

$$\mathcal{U}_{\text{ideal}} = \begin{array}{c} \begin{matrix} 0_I0_S & 0_I1_S & 1_I0_S & 1_I1_S \end{matrix} \\ \begin{bmatrix} 1 & 0 & 0 & 0 \\ 0 & 1 & 0 & 0 \\ 0 & 0 & 0 & 1 \\ 0 & 0 & 1 & 0 \end{bmatrix} \end{array} \begin{matrix} 0_I0_S \\ 0_I1_S \\ 1_I0_S \\ 1_I1_S \end{matrix} \tag{1}$$

In order to characterize the CNOT gate fidelity, we perform partial quantum process tomography (*21, 22*). We prepare two independent initial states, use CNOT gate to operate on them, and then use state tomography to measure the final output states.

(1) The first initial state is the sudden state ρ_1, shown in Matrix (2). Matrix (3) shows the state-tomography result after the CNOT gate is applied.

$$\rho_1 = \begin{array}{c} \begin{matrix} \mathbb{1} & I_x & I_y & I_z \end{matrix} \\ \begin{bmatrix} 0 & 0.014(4) & -0.01(1) & \mathbf{1.763}(7) \\ 0.043(2) & 0.12(2) & -0.15(4) & -0.29(4) \\ 0.030(5) & 0.23(8) & -0.03(2) & 0.16(2) \\ \mathbf{0.460}(6) & 0.04(2) & -0.085(9) & -0.12(3) \end{bmatrix} \end{array} \begin{matrix} \mathbb{1} \\ S_x \\ S_y \\ S_z \end{matrix} , \tag{2}$$

$$\rho_1^{\text{CNOT}} = \begin{array}{c} \begin{matrix} \mathbb{1} & I_x & I_y & I_z \end{matrix} \\ \begin{bmatrix} 0 & -0.018(4) & 0.09(2) & \mathbf{1.413}(6) \\ -0.045(4) & -0.08(2) & -0.19(1) & -0.23(4) \\ 0.08(1) & -0.10(3) & -0.13(1) & -0.089(8) \\ -0.032(7) & 0.14(2) & -0.18(1) & \mathbf{0.80}(3) \end{bmatrix} \end{array} \begin{matrix} \mathbb{1} \\ S_x \\ S_y \\ S_z \end{matrix} \tag{3}$$

which can be rewritten in the computational basis

$$\rho_1 = \begin{array}{c} \begin{matrix} 0_I0_S & 0_I1_S & 1_I0_S & 1_I1_S \end{matrix} \\ \begin{bmatrix} 1.08 & -0.05 - 0.06\text{i} & 0.018 + 0.026\text{i} & 0.036 - 0.020\text{i} \\ -0.05 + 0.06\text{i} & 0.68 & 0.023 + 0.095\text{i} & -0.0033 - 0.017\text{i} \\ 0.018 - 0.026\text{i} & 0.023 - 0.095\text{i} & -0.62 & 0.094 + 0.025\text{i} \\ 0.036 + 0.020\text{i} & -0.0033 + 0.017\text{i} & 0.094 - 0.025\text{i} & -1.14 \end{bmatrix} \end{array} \begin{matrix} 0_I0_S \\ 0_I1_S \\ 1_I0_S \\ 1_I1_S \end{matrix} \tag{4}$$

$$\rho_1^{\text{CNOT}} = \begin{array}{c} \begin{matrix} 0_I0_S & 0_I1_S & 1_I0_S & 1_I1_S \end{matrix} \\ \begin{bmatrix} 0.89 & -0.080 - 0.020\text{i} & 0.027 + 0.002\text{i} & 0.013 + 0.072\text{i} \\ -0.080 + 0.020\text{i} & 0.52 & -0.053 + 0.023\text{i} & -0.045 - 0.090\text{i} \\ 0.027 - 0.002\text{i} & -0.053 - 0.023\text{i} & -0.92 & 0.035 - 0.064\text{i} \\ 0.013 - 0.072\text{i} & -0.045 + 0.090\text{i} & 0.035 + 0.064\text{i} & -0.49 \end{bmatrix} \end{array} \begin{matrix} 0_I0_S \\ 0_I1_S \\ 1_I0_S \\ 1_I1_S \end{matrix} \tag{5}$$

(2) The second initial state is ρ_2, which is prepared by applying $[\frac{\pi}{2}]_I^x$ on the imperfect sudden state. After implementing CNOT gate on ρ_2, the state becomes ρ_2^{CNOT}. The state-tomography results of ρ_2 and ρ_2^{CNOT} are

$$\rho_2 = \begin{array}{c} \begin{matrix} \mathbb{1} & I_x & I_y & I_z \end{matrix} \\ \begin{bmatrix} 0 & -0.41(1) & \mathbf{1.32}(3) & -0.069(4) \\ 0.137(7) & -0.25(2) & 0.15(2) & -0.22(1) \\ -0.016(5) & \mathbf{0.47}(7) & -0.025(9) & -0.27(2) \\ \mathbf{0.34}(1) & 0.28(2) & 0.253(9) & -0.25(1) \end{bmatrix} \end{array} \begin{matrix} \mathbb{1} \\ S_x \\ S_y \\ S_z \end{matrix},$$

$$\rho_2^{\text{CNOT}} = \begin{array}{c} \begin{matrix} \mathbb{1} & I_x & I_y & I_z \end{matrix} \\ \begin{bmatrix} 0 & 0.21(1) & -0.208(7) & 0.147(9) \\ 0.133(6) & -1.48(4) & \mathbf{2.40}(5) & 1.01(5) \\ -0.131(9) & -0.01(1) & 0.20(2) & -0.41(2) \\ 0.038(6) & 0.10(4) & \mathbf{0.46}(2) & \mathbf{0.57}(5) \end{bmatrix} \end{array} \begin{matrix} \mathbb{1} \\ S_x \\ S_y \\ S_z \end{matrix}$$

Considering the high-fidelity performance of single-spin gates, the unknown $\mathcal{U}_{\text{CNOT}}$ is assumed to be a unitary matrix. In addition, it is reasonable to assume: $\mathcal{U}_{\text{CNOT}}(1,1) \geq 0, \mathcal{U}_{\text{CNOT}}(2,2) \geq 0, \mathcal{U}_{\text{CNOT}}(3,4) \geq 0$, and $\mathcal{U}_{\text{CNOT}}(4,3) \geq 0$. This assumption is used to determine the coordinate orientation of CNOT gate. Additionally, some prior information can be used, i.e., the magnetic-field pulse directions, which are calibrated with a flux-gate magnetometer. Based on the experimental information and prior assumptions of the CNOT gate, the actual CNOT gate $\mathcal{U}_{\text{CNOT}}$ is numerically reconstructed by using a constrained fitting technique

$$\min_{\mathcal{U}_{\text{CNOT}}} \; k_1 \cdot ||\mathcal{B}_1||_l + k_2 \cdot ||\mathcal{B}_2||_l,$$

subject to

$$\mathcal{B}_1 = \mathcal{U}_{\text{CNOT}}\rho_1\mathcal{U}_{\text{CNOT}}^{\dagger} - \rho_1^{\text{CNOT}}, \mathcal{B}_2 = \mathcal{U}_{\text{CNOT}}\rho_2\mathcal{U}_{\text{CNOT}}^{\dagger} - \rho_2^{\text{CNOT}},$$
$$\mathcal{U}_{\text{CNOT}}(i,j) \in \mathbb{R}, \text{ and } \mathcal{U}_{\text{CNOT}}\mathcal{U}_{\text{CNOT}}^{\dagger} = \mathbb{1},$$
$$\mathcal{U}_{\text{CNOT}}(i,j) \geq 0 \text{ when } (i,j) = (1,1),(2,2),(3,4),(4,3)$$

where k_1 and k_2 are real weighting factors of $||\mathcal{B}_1||_l$ and $||\mathcal{B}_2||_l$. $||\cdot||_l$ represents the l-norm of a matrix, $||\mathcal{B}_1||_l$ and $||\mathcal{B}_2||_l$ are calculated according to the definition of l-norm, i.e., $||\mathcal{B}||_1 = \max_j \sum_{i=1}^4 |\mathcal{B}_{ij}|$ (1-norm), $||\mathcal{B}||_F = (\sum_i^4 \sum_j^4 |\mathcal{B}_{ij}|^2)^{1/2}$ (F-norm) and $||\mathcal{B}||_\infty = \max_i \sum_{j=1}^4 |\mathcal{B}_{ij}|$ (∞-norm). In this work, three different l-norms are exploited in the constrained fitting, as shown in table S4. Two weighting factors k_1 and k_2 are introduced to adjust weights of contributions of the two CNOT gate experiments. When the final result of CNOT gate in the computational basis is obtained, the gate fidelity is directly calculated as $f = \frac{1}{4}\text{Tr}[\mathcal{U}_{\text{ideal}}^T\mathcal{U}_{\text{CNOT}}]$. table S4 shows that the fidelities of CNOT gate are all close 0.99 according to the three different l-norms. When $k_1 = 2$ and $k_2 = 1$, the $k_1 \cdot ||\mathcal{B}_1||_l$ and $k_2 \cdot ||\mathcal{B}_2||_l$ are close to each other. In detail, the CNOT-gate matrices with three different l-norms are close, thus we can choose one of the three cases as the CNOT gate. For example, we choose the results based on F-norm as the CNOT gate with an estimated fidelity of $0.9877(2)$, where

$$\mathcal{U}_{\text{CNOT}} = \begin{array}{c} \begin{matrix} 0_I0_S & 0_I1_S & 1_I0_S & 1_I1_S \end{matrix} \\ \begin{bmatrix} 0.9900 & 0.1112 & -0.0489 & -0.0715 \\ -0.1074 & 0.9928 & 0.0456 & 0.0262 \\ 0.0663 & -0.0128 & -0.1327 & 0.9889 \\ 0.0628 & -0.0420 & 0.9889 & 0.1279 \end{bmatrix} \end{array} \begin{matrix} 0_I0_S \\ 0_I1_S \\ 1_I0_S \\ 1_I1_S \end{matrix}$$

table S1. The evolutions of two-spin operators under the scalar spin-spin coupling.

Spin operator $I_\nu S_\mu$	$\mathcal{U}_J I_\nu S_\mu \mathcal{U}_J^\dagger$, with $\mathcal{U}_J = e^{-iH_J t}$
I_x	$\cos^2(\pi Jt)I_x + \sin^2(\pi Jt)S_x + (I_yS_z - I_zS_y)\sin(2\pi Jt)$
I_y	$\cos^2(\pi Jt)I_y + \sin^2(\pi Jt)S_y - (I_xS_z - I_zS_x)\sin(2\pi Jt)$
I_z	$\cos^2(\pi Jt)I_z + \sin^2(\pi Jt)S_z + (I_xS_y - I_yS_x)\sin(2\pi Jt)$
S_x	$\cos^2(\pi Jt)S_x + \sin^2(\pi Jt)I_x + (I_zS_y - I_yS_z)\sin(2\pi Jt)$
S_y	$\cos^2(\pi Jt)S_y + \sin^2(\pi Jt)I_y - (I_zS_x - I_xS_z)\sin(2\pi Jt)$
S_z	$\cos^2(\pi Jt)S_z + \sin^2(\pi Jt)I_z + (I_yS_x - I_xS_y)\sin(2\pi Jt)$
I_xS_y	$\cos^2(\pi Jt)I_xS_y + \sin^2(\pi Jt)I_yS_x - \frac{1}{4}(I_z - S_z)\sin(2\pi Jt)$
I_yS_x	$\cos^2(\pi Jt)I_yS_x + \sin^2(\pi Jt)I_xS_y + \frac{1}{4}(I_z - S_z)\sin(2\pi Jt)$
I_xS_x	I_xS_x
I_yS_y	I_yS_y
I_zS_z	I_zS_z
I_xS_z	$\cos^2(\pi Jt)I_xS_z + \sin^2(\pi Jt)I_zS_x + \frac{1}{4}(I_y - S_y)\sin(2\pi Jt)$
I_zS_x	$\cos^2(\pi Jt)I_zS_x + \sin^2(\pi Jt)I_xS_z - \frac{1}{4}(I_y - S_y)\sin(2\pi Jt)$
I_yS_z	$\cos^2(\pi Jt)I_yS_z + \sin^2(\pi Jt)I_zS_y - \frac{1}{4}(I_x - S_x)\sin(2\pi Jt)$
I_zS_y	$\cos^2(\pi Jt)I_zS_y + \sin^2(\pi Jt)I_yS_z + \frac{1}{4}(I_x - S_x)\sin(2\pi Jt)$

table S2. Temporal averaging sequences for state tomography.

Each $I_\nu S_\mu$ term is the averaged results of four independent experiments with preparation operation $\mathcal{P}_i,\ i = 1, 2, 3, 4$. θ_S^η, θ_I^η denote rotations by angle θ along η for spin $\mathbf{S}$ and spin $\mathbf{I}$, respectively. $\pi_I^x - \pi_S^z$ denotes applying π_S^z at first and then applying π_I^x. Similarly for other pulses.

$I_\nu S_\mu$	$\mathcal{P}_1$	$\mathcal{P}_2$	$\mathcal{P}_3$	$\mathcal{P}_4$
S_z	no operation	π_S^z	π_I^x	$\pi_I^x - \pi_S^z$
I_z	no operation	π_I^z	π_S^x	$\pi_I^z - \pi_S^x$
I_xS_y	no operation	π_S^y	$\pi_I^y - \pi_S^z$	$\pi_I^y - \pi_S^x$
I_yS_x	no operation	π_S^x	$\pi_I^x - \pi_S^y$	$\pi_I^x - \pi_S^z$
S_x	$[\frac{\pi}{2}]_S^y$	$\pi_S^z - [\frac{\pi}{2}]_S^y$	$\pi_I^x - [\frac{\pi}{2}]_S^y$	$\pi_I^x - \pi_S^z - [\frac{\pi}{2}]_S^y$
S_y	$[\frac{\pi}{2}]_S^x$	$\pi_S^z - [\frac{\pi}{2}]_S^x$	$\pi_I^x - [\frac{\pi}{2}]_S^x$	$\pi_I^x - \pi_S^z - [\frac{\pi}{2}]_S^x$
I_x	$[\frac{\pi}{2}]_I^y$	$\pi_I^z - [\frac{\pi}{2}]_I^y$	$\pi_S^x - [\frac{\pi}{2}]_I^y$	$\pi_I^z - \pi_S^x - [\frac{\pi}{2}]_I^y$
I_y	$[\frac{\pi}{2}]_I^x$	$\pi_I^z - [\frac{\pi}{2}]_I^x$	$\pi_S^x - [\frac{\pi}{2}]_I^x$	$\pi_I^z - \pi_S^x - [\frac{\pi}{2}]_I^x$
I_xS_x	$[\frac{\pi}{2}]_S^z$	$\pi_S^y - [\frac{\pi}{2}]_S^z$	$\pi_I^y - \pi_S^z - [\frac{\pi}{2}]_S^z$	$\pi_I^y - \pi_S^x - [\frac{\pi}{2}]_S^z$
I_xS_z	$[\frac{\pi}{2}]_S^x$	$\pi_S^y - [\frac{\pi}{2}]_S^x$	$\pi_I^y - \pi_S^z - [\frac{\pi}{2}]_S^x$	$\pi_I^y - \pi_S^x - [\frac{\pi}{2}]_S^x$
I_yS_y	$[\frac{\pi}{2}]_S^z$	$\pi_S^x - [\frac{\pi}{2}]_S^z$	$\pi_I^x - \pi_S^y - [\frac{\pi}{2}]_S^z$	$\pi_I^x - \pi_S^z - [\frac{\pi}{2}]_S^z$
I_yS_z	$[\frac{\pi}{2}]_S^y$	$\pi_S^x - [\frac{\pi}{2}]_S^y$	$\pi_I^x - \pi_S^y - [\frac{\pi}{2}]_S^y$	$\pi_I^x - \pi_S^z - [\frac{\pi}{2}]_S^y$
I_zS_x	$[\frac{\pi}{2}]_I^x$	$\pi_S^x - [\frac{\pi}{2}]_I^x$	$\pi_I^x - \pi_S^y - [\frac{\pi}{2}]_I^x$	$\pi_I^x - \pi_S^z - [\frac{\pi}{2}]_I^x$
I_zS_y	$[\frac{\pi}{2}]_I^y$	$\pi_S^y - [\frac{\pi}{2}]_I^y$	$\pi_I^y - \pi_S^z - [\frac{\pi}{2}]_I^y$	$\pi_I^y - \pi_S^x - [\frac{\pi}{2}]_I^y$
I_zS_z	$[\frac{\pi}{2}]_I^y - [\frac{\pi}{2}]_S^x$	$\pi_S^y - [\frac{\pi}{2}]_I^y - [\frac{\pi}{2}]_S^x$	$\pi_I^y - \pi_S^z - [\frac{\pi}{2}]_I^y - [\frac{\pi}{2}]_S^x$	$\pi_I^y - \pi_S^x - [\frac{\pi}{2}]_I^y - [\frac{\pi}{2}]_S^x$

table S3. The evolution of the two-spin operators under the CNOT gate.

$I_\nu S_\mu$	$\mathcal{U}_{\text{CNOT}} I_\nu S_\mu \mathcal{U}_{\text{CNOT}}^\dagger$	$I_\nu S_\mu$	$\mathcal{U}_{\text{CNOT}} I_\nu S_\mu \mathcal{U}_{\text{CNOT}}^\dagger$	$I_\nu S_\mu$	$\mathcal{U}_{\text{CNOT}} I_\nu S_\mu \mathcal{U}_{\text{CNOT}}^\dagger$
I_x	$2I_xS_x$	S_x	S_x	I_xS_x	$\frac{1}{2}I_x$
I_y	$2I_yS_x$	S_y	$2I_zS_y$	I_yS_y	$-I_xS_z$
I_z	I_z	S_z	$2I_zS_z$	I_zS_z	$\frac{1}{2}S_z$
I_xS_y	I_yS_z	I_xS_z	$-I_yS_y$	I_yS_x	$\frac{1}{2}I_y$
I_yS_z	I_xS_y	I_zS_x	I_zS_x	I_zS_y	$\frac{1}{2}S_y$

table S4. Reconstructing the CNOT gate based on l-norm.

Here $||\mathcal{B}_1||_l$ and $||\mathcal{B}_2||_l$ are calculated according to the definition of l-norm: $||\mathcal{B}||_1 = \max_j \sum_{i=1}^{4} |\mathcal{B}_{ij}|$ (1-norm), $||\mathcal{B}||_F = (\sum_i^4 \sum_j^4 |\mathcal{B}_{ij}|^2)^{1/2}$ (F-norm) and $||\mathcal{B}||_\infty = \max_i \sum_{j=1}^{4} |\mathcal{B}_{ij}|$ (∞-norm).

k_1,k_2	fidelity	$k_1 \cdot \|\|\mathcal{B}_1\|\|_1$	$k_2 \cdot \|\|\mathcal{B}_2\|\|_1$	$k_1 \cdot \|\|\mathcal{B}_1\|\|_1 + k_2 \cdot \|\|\mathcal{B}_2\|\|_1$
$1, 1$	$0.9894(3)$	0.4398	0.9812	1.4210
$2, 1$	$0.9922(3)$	0.8600	0.9925	1.8525
$3, 1$	$0.9939(3)$	1.2766	1.0042	2.2808

k_1,k_2	fidelity	$k_1 \cdot \|\|\mathcal{B}_1\|\|_F$	$k_2 \cdot \|\|\mathcal{B}_2\|\|_F$	$k_1 \cdot \|\|\mathcal{B}_1\|\|_F + k_2 \cdot \|\|\mathcal{B}_2\|\|_F$
$1, 1$	$0.9808(4)$	0.4808	0.8977	1.3785
$2, 1$	$0.9877(2)$	0.9201	0.9176	1.8377
$3, 1$	$0.9897(2)$	1.3650	0.9313	2.2963

k_1,k_2	fidelity	$k_1 \cdot \|\|\mathcal{B}_1\|\|_\infty$	$k_2 \cdot \|\|\mathcal{B}_2\|\|_\infty$	$k_1 \cdot \|\|\mathcal{B}_1\|\|_\infty + k_2 \cdot \|\|\mathcal{B}_2\|\|_\infty$
$1, 1$	$0.9894(4)$	0.4408	0.9788	1.4196
$2, 1$	$0.9922(3)$	0.8567	1.0000	1.8567
$3, 1$	$0.9934(3)$	1.2788	1.0057	2.2845

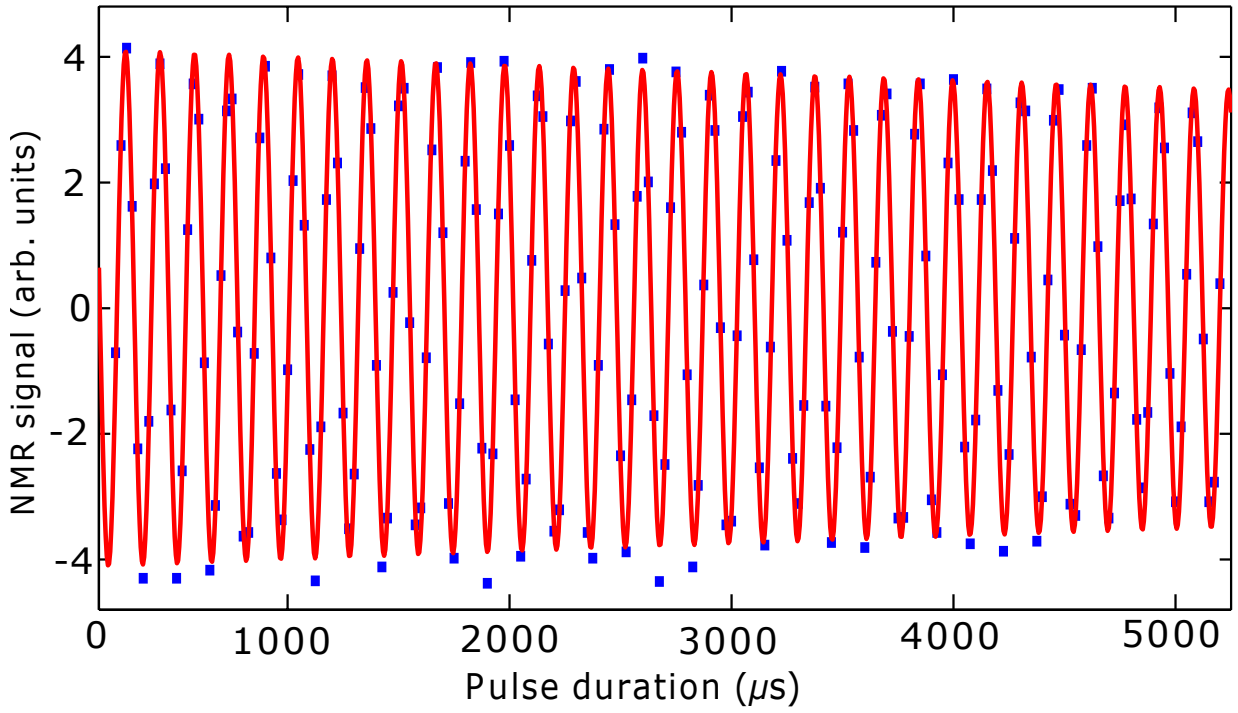

fig. S2. Dependence of NMR signal amplitude on z pulse duration. The amplitude of the magnetic-field pulse is kept constant during the measurement. The line is a fit to function $ae^{-t/T}\sin(2\pi ft + b)$ with $a = 4.1$, $T = 3.1 \times 10^{-2}$ s, $f = 6.4 \times 10^{3}$ Hz, and $b = -3.1$ rad. The magnetic-field inhomogeneity of the magnetic field pulse around the sample can be estimated as $(\pi fT)^{-1} \approx 0.2\%$.